ISSN 0023-1584, Kinetics and Catalysis, 2009, Vol. 50, No. 2, pp. 304–313. © Pleiades Publishing, Ltd., 2009.
Original Russian Text © V.V. Gorodetskii, 2009, published in Kinetika i Kataliz, 2009, Vol. 50, No. 2, pp. 322–331.

FIFTY YEARS
OF THE BORESKOV INSTITUTE OF CATALYSIS

Experimental Evidence of Propagating Waves in Hydrogen Oxidation on Platinum-Group Metals (Pt, Rh, Ir)

V. V. Gorodetskii

Boreskov Institute of Catalysis, Siberian Branch, Russian Academy of Sciences, Novosibirsk, 630090 Russia
e-mail: gorodetsk@catalysis.ru

Received March 28, 2008

Abstract—The $H_{2(g)} + O_{ads}$ reaction on nanoplanes of Pt-, Rh- and Ir-tips with a radius of ~10^3 Å was studied by FEM with a resolution of ~20 Å, and the critical conditions (P_i, T) under which this reaction is accompanied by the formation of a propagating wave front with a sharp boundary between the H_{ads}- and O_{ads}-layers were determined. The $H_2 + O_2$ reaction on a Pt-tip under steady-state conditions was studied by FIM with a lateral atomic resolution of ~5 Å, and images of H_2O molecules (H_2O^+ ions) visualizing the spatial distribution of catalytically active sites (platinum atoms) were obtained for the first time. The origin of the kinetic self-oscillations in isothermal H_2 oxidation in situ was investigated in detail. The regular chemical waves were found to be initiated by the reversible phase transition (Pt(100)-*hex* ⟷ 1 × 1) of the Pt(100) nanoplane surface. A stepwise H_2O formation mechanism involving OH_{ads}-groups was deduced from HREELS and TDS for the $H_{ads} + O_{ads}$ reaction on the Pt(111) and Pt(100) single crystal surfaces.

DOI: 10.1134/S0023158409020220

The mechanism of oxidative catalysis by platinum-group metals continues to attract interest because of the possibility of obtaining new experimental and theoretical data elucidating the nature of the active sites and the way in which multiple steady states, self-oscillations, and chemical waves appear. The self-oscillatory phenomena in chemical reactions were observed for the first time in the 1950s for homogeneous catalysis, namely, for the Belousov–Zhabotinsky reaction [1]. Using this reaction as an example, Nicolis and Prigogine [2] created the theory of the complex dynamic behavior of chemical systems far from thermodynamic equilibrium. The concept of a dissipative structure (stable regular structure) was suggested, which means the spatial and temporal self-organization of reacting species. In heterogeneous catalysis, dissipative structures manifest themselves as traveling concentration waves, whose extent is determined by the diffusion and reactivity of the reacting species. It was demonstrated that the self-oscillatory mode is possible only upon reaching the critical reaction conditions (P_i, T).

Although nonlinear phenomena are very difficult to investigate experimentally because of their great sensitivity to external actions, their character has been studied in detail at the macroscopic level for the $CO + O_2$, $NO + H_2$, $NO + NH_3$, and NO + CO reactions on Pt, Pd, and Rh single crystal surfaces. Different mechanisms of the appearance of self-oscillations and surface waves were discovered and studied. These are a surface phase transition ($CO + O_2$/Pt(100): (*hex*) ⟷ (1 × 1)), the formation of a "subsurface" oxygen layer ($CO + O_2$/Pd(110)), and the "explosive" interaction between adsorbed species ($NO + H_2$/Pt(100)) [3, 4]. A common feature of all these mechanisms is the spontaneous periodical transitions of the metal from an inactive to a highly active state.

Since the concept of active sites was suggested in the 1930s, there have been many attempts to study the structure and properties of active sites at the microscopic level. The development of photoemission electron microscopy made it possible to observe, in the early 1990s, the formation of chemical waves on the Pt and Pd single crystal surfaces under conditions of isothermal oscillations of reaction rates—a new, previously unknown phenomenon. For example, for the reaction $CO + O_2$/Pt(110), the regular propagation of the reaction fronts of O_{ads} and CO_{ads} adsorbed layers was observed visually at a spatial resolution of ~1 μm [3, 4]. Passing to the atomic level in the investigation of active sites is possible only using the scanning tunneling microscopy and field ion microscopy techniques. Among the methods, only field ion microscopy (FIM) seems to be suitable for real-time in situ studies of the dynamics of surface processes on a single microcrystallite (sharp tip) ~10^3 Å in size with near-atomic resolution. For the first time, the formation of a traveling wave was observed in the early 1970s in our studies of the $H_{2(g)} + O_{ads}$ titration reaction on the Pt-, Ir- and Rh-tip surfaces using field emission microscopy (FEM) with a resolution of ~20 Å [5–7]. Using the FIM method, which makes possible real-time visual in situ observations of the surface dynamic processes with a spatial

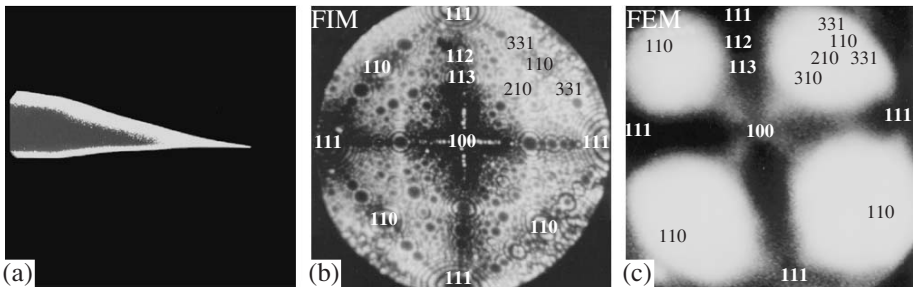

Fig. 1. (a) Transmission electron micrograph of the Pt-tip. (b) FIM-image of the [100]-oriented Pt-tip with a radius of ~700 Å obtained using Ne^+ as the imaging gas: $T = 78$ K, $F = 3.5$ V/Å, $V_{FIM} = 15$ kV, $P_{Ne} = 2 \times 10^{-4}$ mbar. Each spot in the image represents a separate platinum atom. (c) FEM image of the same surface of the Pt-tip: $V_{FEM} = -2.5$ kV, $F = 0.3$ V/Å.

resolution of ~5 Å, we were the first to pass to the near-atomic level in the investigation of H_2 and CO oxidation on platinum [8, 9].

The platinum-group metals (Pt, Rh, Ir) are known to be very active in the catalytic oxidation of hydrogen [10]. Among the mechanisms suggested for H_2 oxidation [11, 12], the Langmuir–Hinshelwood (L–H) stepwise mechanism involving hydroxyl groups (OH_{ads}) seems to be the most likely. Upon adsorption, H_2 and O_2 dissociate into H_{ads}- and O_{ads}-atoms [11–13]. The formation of H_2O molecules can be represented as the following sequence of steps: $H_{ads} + O_{ads} \longrightarrow OH_{ads}$; $OH_{ads} + H_{ads} \longrightarrow H_2O_{(g)}$ [14, 15].

In the present contribution we report the HREELS, TDS, FEM and FIM results (intermediates, chemical waves) obtained in study: (i) of hydrogen oxidation in situ on the Pt-, Ir- and Rh-tips with a radius of ~10^3 Å; (ii) of reaction mechanism of self-organization on surfaces with dimensions on the order of hundreds angstroms; (iii) of the spontaneous periodical transitions of metal from an inactive to a highly active catalytic state.

METHODS

The FEM and FIM are an experimental tool for performing in situ investigations of real-time dynamic surface processes (surface waves). Ions in the FIM method (electrons in FEM) are accelerated by the applied field from the tip surface (Fig. 1a) towards the detector, which consists of a high-sensitivity microchannel plate and a fluorescent screen [16]. The image is recorded with a CCD video camera.

A high lateral resolution of ~2 Å is achieved in FIM by field ionization of the imaging gas (Ne) over metal atoms at a positive electric field value of $F = 3.5$ V/Å ($Ne \xrightarrow{\text{electric field}} Ne^+ + e^-/Pt$) [16]. Figure 1b shows an image of the Pt-tip surface at a magnification of $\times 2 \times 10^6$ with atomic resolution achieved in Ne^+ at 78 K. Each spot in the image corresponds to a separate platinum atom. This FIM image demonstrates that the hemispherical surface of the sharp Pt-tip with a radius of ~700 Å consists of a number of crystallographically different nanoplanes: densest planes {111}, {110}, and {100}; stepped planes {113} and {331}; and rough planes {210} and {310}. This surface is topographically similar to the surface of the nanocrystallites of a supported metal. Therefore, sharp tips can serve as model systems for solving the "material gap" problem in the study of the nature of active sites in supported metal catalysts. For visual observation of waves on the Pt-tip, we for the first time used the molecules of a reactant (O_2) and the reaction product (H_2O) as the imaging gas in a field of $F \sim 1$–1.5 V/Å [8, 9]. According to the above field ionization mechanism, the resulting water molecules are ionized in a field of $F \sim 1$–1.5 V/Å at a distance of $x_{cr} \sim 4$ Å from the platinum surface via electron tunneling from the ground level of the H_2O molecule to the Fermi level of the metal. The resulting H_2O^+ ions are accelerated toward the screen by a high electric field.

In FEM experiments, a negative voltage V is applied to a Pt-tip. Electrons are emitted into vacuum from the tip by tunneling through a potential barrier by the applied electric field ($F = 0.3$ V/Å) and are accelerated towards a fluorescent screen. The emitted electrons produce an image of the tip surface with ~20-Å resolution at a magnification of $\times 3 \times 10^5$ (Fig. 1c). The surface analysis of the FEM images is based on the changes in local work function ($\Delta\varphi$) accompanying adsorption of H_2 and oxygen, which can be correlated with the total field electron currents according to the Fowler–Nordheim equation. The surface nanoplanes of Pt-tip show an increase of $\Delta\varphi$ with the adsorption of hydrogen ($\Delta\varphi = 0.2$ eV) and an even higher increase after the adsorption of oxygen ($\Delta\varphi = 1.2$ eV). As a consequence, high-contrast dark areas corresponding to the O_{ads}-layer appear on the image [6]. The dramatic decreases in the work function observed in the H_2 oxidation reaction ($\theta_O \longrightarrow \theta_H$) gives an excellent tool for distinguishing transition in the adsorption layers: the oxygen layer with low emission current (dark areas) and hydrogen layer (bright areas) with high emission current [6, 9]. Our studies demonstrated that the electrostatic field used in FEM and FIM does not exert any significant

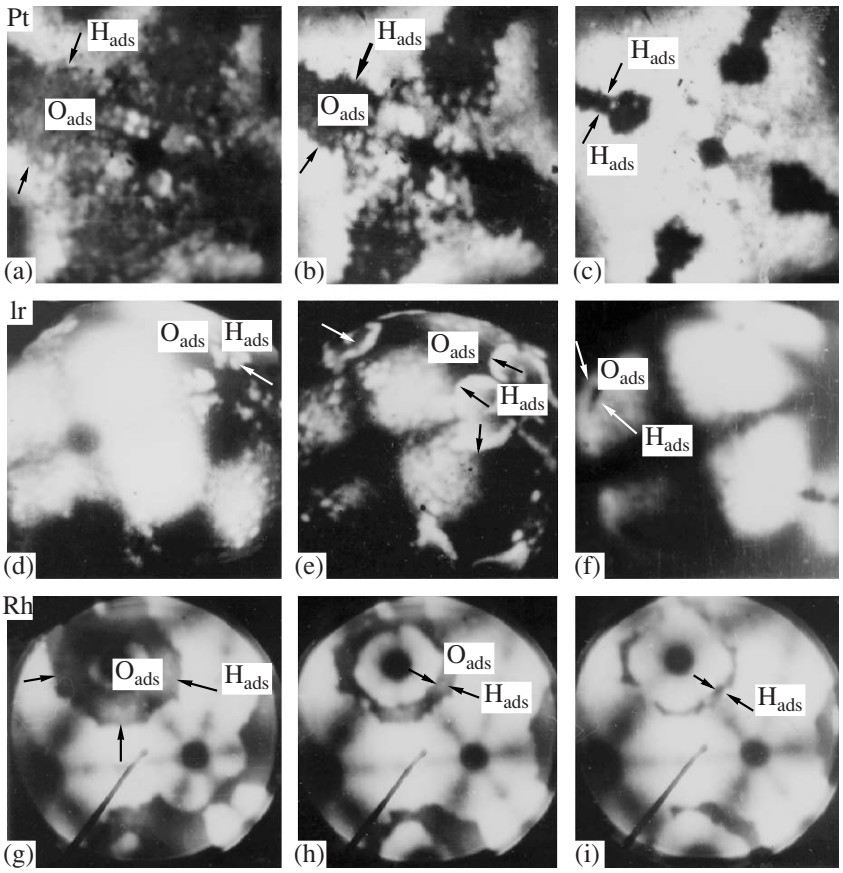

Fig. 2. Formation of O_{ads} islands during wave propagation in the low-temperature reaction $H_2 + O_{ads}$ on the Pt-, Ir- and Rh-tip surfaces. (a–c) Pt: O_2 preadsorption at 78 K and an exposure of 120 L ($\theta_O \sim 1$); $\Delta\varphi = 1.3$ eV; reaction between H_2 and O_{ads} at $T =$ 140 K and $P_{H_2} = 6.5 \times 10^{-6}$ mbar; reaction time of (a) 5, (b) 10, and (c) 25 min. (d–f) Ir: O_2 preadsorption at 78 K and an exposure of 120 L; $\Delta\varphi = 1.2$ eV; reaction between H_2 and O_{ads} at $T =$200 K and $P_{H_2} = 4 \times 10^{-7}$ mbar; reaction time of (d) 2, (e) 4, and (f) 6 min. (g–i) Rh: O_2 preadsorption at 196 K and an exposure of 300 L; $\Delta\varphi = 0.85$ eV; reaction between H_2 and O_{ads} at $T = 280$ K and $P_{H_2} = 2.6 \times 10^{-7}$ mbar; reaction time of (g) 5, (h) 6, and (i) 7 min.

effect on the reactions involving H_2, O_2, CO, or NO molecules, and this finding is in agreement with reports by other authors [17, 18].

Our experiments were carried out using an ultrahigh vacuum (residual pressure of $P_{res} < 10^{-10}$ mbar) setup under flow reactor conditions. The platinum surface was visually observed in situ by the FEM or FIM method [19]. The pressure of the reaction mixture was maintained at a constant value of $\sim 5 \times 10^{-4}$ mbar and was measured with a visco-vac gage and a quadrupole mass spectrometer. The preparation of sharp tips, the cleaning of the tip surface by "field desorption," and the experimental procedure are detailed elsewhere [5–9, 19].

The nature of oxygen and hydrogen adsorption states and reaction intermediates (OH_{ads}-groups) was studied by high resolution electron energy loss spectroscopy (HREELS) and thermal desorption spectroscopy (TDS) that were carried out in the separate ultrahigh vacuum chamber ($P_{res} < 10^{-10}$ mbar) of a VG ADES 400 electron spectrometer [20].

RESULTS AND DISCUSSION

$H_{2(g)} + O_{ads}$ Titration Reaction on Pt, Ir, and Rh-tip Surfaces

The interaction between hydrogen and a preadsorption oxygen layer ($\theta_O \sim 1$) on Pt-, Ir- and Rh-tip surfaces is depicted by the series of FEM images shown in Fig. 2 [21]. The transition from θ_O ($\Delta\varphi \sim 0.9$–1.2 eV) to θ_H ($\Delta\varphi \sim 0.2$–0.4 eV) in the $H_{2(g)} + O_{ads} \longrightarrow H_2O_{(g)} + H_{ads}$ reaction at $T < 300$ K shows itself as the appearance of a mobile reaction boundary that is accompanied by a dramatic decrease in the work function, which is due to the formation and desorption of H_2O molecules. The crystallographic specificity of the Pt-, Ir-, and Rh-tips is illustrated by the series of images in Fig. 2: (a–c) Pt, (d–f) Ir, and (g–i) Rh. On the Pt-tip, oxygen

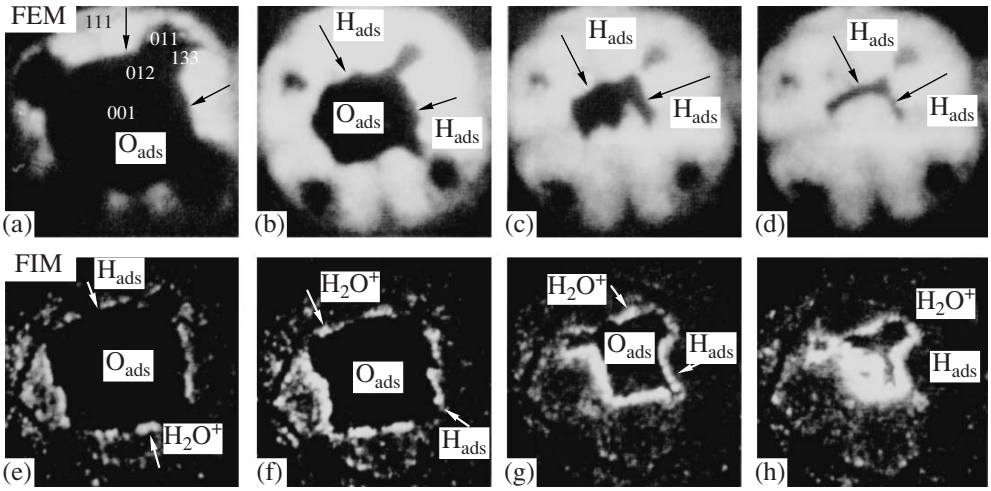

Fig. 3. Propagation of the wave front in the $H_2 + O_{ads}$ reaction on the Pt-tip observed by (a–d) FEM (F = 0.6 V/Å) and (e–h) FIM (H_2O^+, F = 1.5 V/Å). T = 395 K; $P_{H_2} = 4.6 \times 10^{-7}$ mbar; the reaction time is (a) 0, (b) 1.0, (c) 1.3, (d) 1.4, (e) 0, (f) 0.5, (g) 1.3, and (h) 1.5 s. O_2 was preadsorbed at 300 K and an exposure of 10^3 L. $\Delta\varphi$ = 1.2 eV.

adsorbed on the (331) planes and on the stepped planes around (111) is the first to participate in the reaction (Fig. 2a), and this is followed by the involvement of oxygen on the (210) planes (Figs. 2b, 2c). On the Ir-tip, the reaction is initiated on the (321) stepped planes around the (111) plane. This indicated by the appearance of bright spots due to electron emission from the H_{ads}-layer because of the partial removal of the O_{ads}-layer and the corresponding decrease in $\Delta\varphi$ (Fig. 2d). The resulting reaction wave front moves from the (111) planes to the (001) planes, passing rapidly across the stepped planes (112) and (113) (Fig. 2e). The reaction comes to completion on the rough planes (210) and (310), on which unreacted islands of the O_{ads}-layer can still be observed (Fig. 2f, dark spots). For Rh, the sequence of FEM images demonstrates that the transition from the oxygen coverage (O_{ads}, $\Delta\varphi$ = 0.9 eV) to the hydrogen coverage (H_{ads}, $\Delta\varphi$ = 0.4 eV) takes place over approximately 10 min (Figs. 2g–2i). The reaction is initiated on the (110) planes and is accompanied by the formation of isolated oxygen islands (dark spots) on the (100) planes (Fig. 2g). The boundary of the reaction wave propagates simultaneously from the (100) plane to the (111) plane and from the (110) plane to the (100) plane (Fig. 2h). After 7 min, the reaction occurs on the (210) planes, where the formation of isolated oxygen islands (dark spots) can be seen (Fig. 2i).

The above results demonstrate that a characteristic feature of the low-temperature $H_{2(g)} + O_{ads}$ reaction is the formation of a mobile reaction zone with a sharp boundary between the H_{ads} and O_{ads}-layers. Clearly, the interaction between hydrogen and oxygen occurs in an extremely narrow zone (~30 Å) of the propagating wave front. The $H_{2(g)} + O_{ads}$ reaction on Rh begins at a greater temperature (~280 K) than the same reaction on Pt and Ir (140 and 200 K).The oxygen layers on the stepped planes $(100)_{st}$ and $(110)_{st}$ are initially involved in the reaction. The reaction occurs between mobile hydrogen atoms (H_{ads}) and an immobile layer of oxygen atoms (O_{ads}) that is characterized by the formation of isolated oxygen islands. The activity order of Rh nanoplanes is as follows: $(100)_{st}$ ~ (110) > (311) > $(111)_{st}$ ~ (111) > (210). Another activity order is observed for platinum: (331) > (111) > (110) > $(100)_{st}$ > (210). For iridium: (321) > (111) > (110) > $(100)_{st}$ > (210). The lowest activity of the rough nanoplane (210) for Pt, Rh, and Ir is likely explained by the fact that this nanoplane forms stronger bonds with adsorbed oxygen atoms than the densest plane (111) or (100). It was demonstrated that the $H_{ads} + O_{ads}$ reaction in a mixed layer is characterized by an apparent activation energy of ~8 kJ/mol [21].

Imaging of the Reaction Wave Front Using the Reaction Product (H_2O Molecules)

Figure 3 presents a series of (a–d) FEM and (e–h) FIM images depicting the origination and propagation of the wave front in the $H_{2(g)} + O_{ads} \longrightarrow H_2O_{(g)} + H_{ads}$ reaction on platinum for a reaction time of τ ~ 1.5 s at T = 395 K [22]. Clearly defined anisotropy is observed in the propagation of the wave front in the direction $\{111\} \longrightarrow \{011\} \longrightarrow \{113\} \longrightarrow \{001\} \longrightarrow \{012\}$. The oxygen island formed on the planes (001) and (012) (see Fig. 3a or Fig. 3e) diminishes along the boundary of the adsorbed O_{ads}-layer (Figs. 3b–3d). The same titration reaction has also been studied by FIM for the first time. An extremely narrow reaction front is imaged here by H_2O^+ ions being formed near the Pt-tip surface from the desorbing reaction product: $H_2O_{(g)} \xrightarrow{\text{field}} H_2O^+ + e^-$ (Figs. 3e–3h). The high local

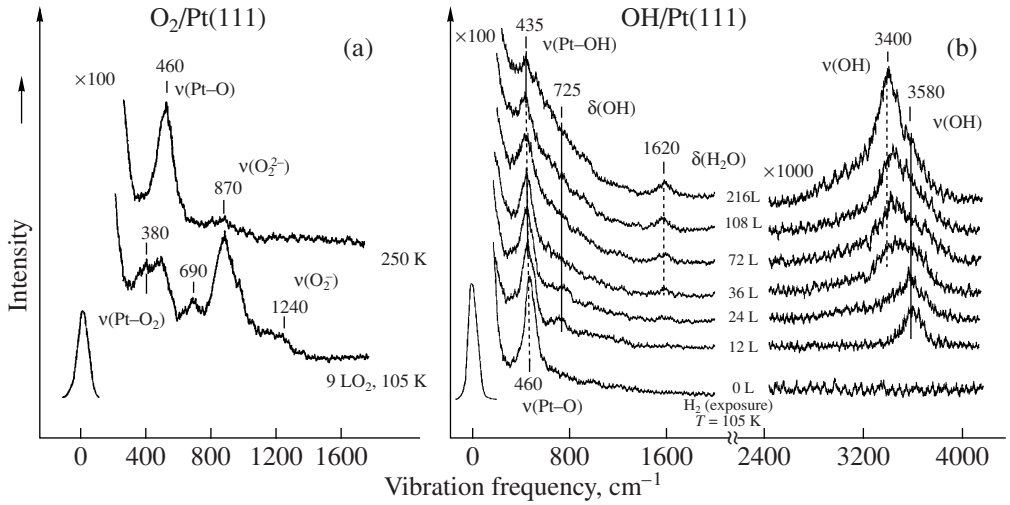

Fig. 4. (a) Evolution of the electron energy loss spectra during the $H_2 + O_{ads}$ reaction on the Pt(100) plane at $T = 105$ K. The layer of oxygen atoms was obtained by low-temperature O_2 adsorption ($T = 105$ K, 9 L) followed by heating to 250 K. (b) Formation of OH_{ads} hydroxyl groups (H_2 exposure of ~12 L) and H_2O_{ads} molecules (H_2 exposure of ~24–216 L).

space resolution achieved in this method (~5 Å) makes possible real-time identification of active sites on the platinum surface at a near-atomic level.

Detection of the Intermediate: OH_{ads} Hydroxyl Group

The spectroscopic data [14, 15, 24] reveal that two independent pathways for water formation via reaction of adsorbed hydrogen with the adsorbed hydroxyl ($H_{ads} + O_{ads} \longrightarrow OH_{ads}$, $OH_{ads} + H_{ads} \longrightarrow H_2O_{(g)}$) or via hydroxyl disproportionation ($2OH_{ads} \longrightarrow H_2O_{(g)} + O_{ads}$) that could be considered viable for the platinum-group metals.

At studying the mechanism of low-temperature H_2 oxidation on the Pt(111) surface, the following results have been observed: (1) the reaction effectively proceeds at $T < 150$ K [14, 25]; (2) H_2 adsorption on the vacant centers in oxygen adsorbed layer (O_{ads}/Pt) is dissociative [26]; (3) H_2O adsorption is molecular on a clean surface, but proceeds with dissociation ($H_2O_{ads} + O_{ads} \longrightarrow 2OH_{ads}$) on the oxygen layer ($O_{ads}$/Pt) [27]; (4) the formation of OH-groups is result of the H_{ads} and O_{ads} interaction [14, 25]. The spectroscopic evidence for the formation of OH-groups is based on the occurrence of deformation vibrations δ(Pt–OH) at 790 cm^{-1} [14] or, on other data [25], their occurrence has been observed at 970 cm^{-1}. Note that the spectra [14, 25] do not show ν(OH) stretching bands for OH_{ads}-groups. The difference between the observed values of the δ(Pt–OH) band (180 cm^{-1}) is likely due to the presence of CO_{ads} or H_2O_{ads} molecules on the Pt(111) surface [14, 25], which are capable of shifting the bending band of the OH_{ads}-group.

In our spectroscopic study, the special attention was given to vacuum conditions ($P_{res} < 3 \times 10^{-11}$ mbar), excluding the low temperature H_2O or CO adsorption on platinum from residual gas [23].

The $H_{2(g)} + O_{ads} \longrightarrow H_2O_{ads} + H_{ads}$ reaction on the Pt(111) surface at $T = 105$ K was studied by HREELS. The vibrational spectrum of the H_{ads}-layer on the Pt(111) surface contains ν(Pt–H) stretching bands at 500 and 1200 cm^{-1} [28]. A precovered atomic oxygen layer with $\theta_O = 0.25$ in the structure $p(2 \times 2)$ was carried out by a technique [29].According to HREELS data, oxygen adsorption on Pt(111) at 105 K results in the formation of two molecular species, namely, the peroxide species O_{2ads}^{2-}, characterized by a ν(O–O) band at 870 cm^{-1} and a ν(Pt–O_2) band at 380 cm^{-1}, and the superoxide species O_{2ads}^{-}, characterized by a ν(O–O) band at 1240 cm^{-1} Heating up ($T \sim 105$–250 K) causes the transition of molecular oxygen to an atomic state characterized by a ν(Pt–O) band at 460 cm^{-1} (Fig. 4a) and O_{2ads} desorption at 160 K.

The O_{ads}-layer is characterized by an intense ν(Pt–O) stretching band at 460 cm^{-1} (Fig. 4a). The proposed technique allows to keep a high concentration of the empty sites, which is necessary for subsequent dissociation of H_2 on an O/Pt(111) surface. As follows from the series of spectra presented in Fig. 4b, the initial stage of the reaction, $H_{ads} + O_{ads} \longrightarrow OH_{ads}$ (H_2, 12 L), is accompanied by the formation of hydroxyl groups with a ν(O–H) stretching band at 3580 cm^{-1} and a δ(Pt–OH) deformation band at 725 cm^{-1}. Simultaneously, a ν(Pt–OH) stretching band as a shoulder appears at a low frequency of 435 cm^{-1}. Note that the presence of the ν(O–H) band at 3580 cm^{-1} is character-

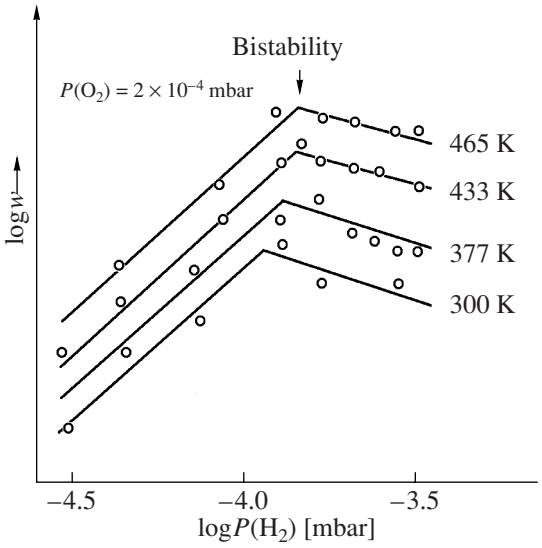

Fig. 5. Rate of hydrogen oxidation on the Pt-tip as a function of the hydrogen partial pressure at $P_{O_2} = 2 \times 10^{-4}$ mbar and T = 300–465 K (FIM data).

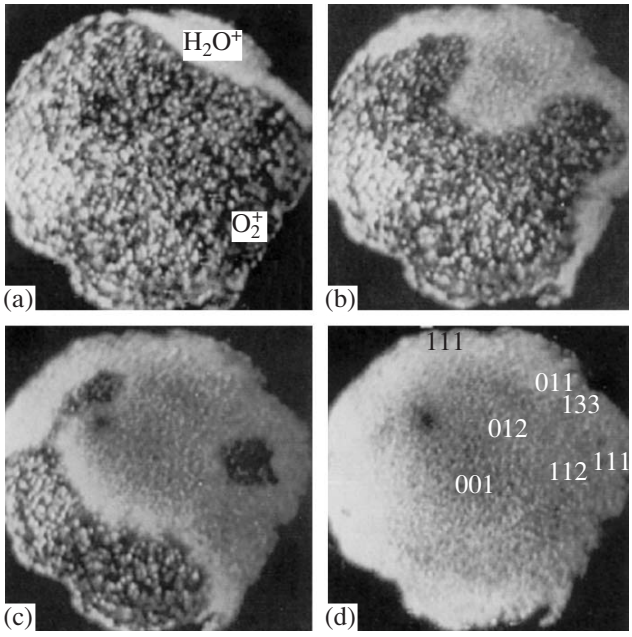

Fig. 6. FIM images showing different stages (a–d) in the wave propagation during the H_2 oxidation over O_{ads}-side precovered surface at the transition ($\theta_O \longrightarrow \theta_H$) point. T = 300 K; $P_{O_2} = 2 \times 10^{-4}$ mbar; $P_{H_2} = 6 \times 10^{-4}$ mbar; reaction time of (a) 0, (b) 0.12, (c) 0.15, and (d) 0.36 s.

istic of isolated OH_{ads} groups, whose formation was observed earlier on the Ag(111) plane as a band at 3640 cm^{-1} [30]. In the second stage of the H_{ads} + $OH_{ads} \longrightarrow H_2O_{ads}$ reaction (H_2, 24–100 L), the beginning of the formation of the H_2O_{ads} layer occurs with the frequencies of deformation vibrations δ(HOH) at 1620 cm^{-1}. Simultaneously the high-frequency area δ(O–H) is accompanied by displacement on 60–100 cm^{-1} up to value of 3400 cm^{-1} that is responsible for adsorbed water molecules layer. Disappearance of deformation vibrations δ(Pt–OH) at 725 cm^{-1} is also observed.

At an H_2 exposure of ~100 L, the preadsorbed O_{ads}-layer is almost entirely converted into an H_2O_{ads}-layer. The *S*-shaped character of intensity vibrations δ(HOH) suggests that the reaction H_{ads} + $O_{ads} \longrightarrow OH_{ads} + H_{ads} \longrightarrow H_2O_{ads}$ should be proportional to borderline of oxygen islands O_{ads}, which is in agreement with FEM and FIM data (Fig. 3).

Steady-State Kinetics of the Reaction

The steady-state reaction rate was measured on a platinum wire used as the Pt-tip holder. The gas phase was analyzed by mass spectrometry. Simultaneously, the composition of the adsorbed layer (O_{ads} or H_{ads}) was monitored by in situ FEM measurements of the work function [21]. The apparent activation energy of the reaction (E_a) at T ~ 180–250 K was ~13 kJ/mol. FEM data indicate that, in the steady-state of the reaction ($P_{H_2}/P_{O_2} = 2:1$, T = 180–250 K), the Pt surface is covered with an H_{ads}-layer. Figure 5 plots the rate of H_2 oxidation (H_2O formation) on a Pt-tip (FIM data) at T > 300 K (T ~ 300–465 K, $P_{O_2} = 2 \times 10^{-4}$ mbar) as a function of the hydrogen partial pressure in the reaction system. This kind of kinetics (the break of the log$w$ curve and the order of the reaction with respect to P_{H_2}) is in agreement with the kinetic data obtained for platinum single crystals [31]. As measured by FIM, E_a at T < 300 K (T ~ 200–300 K, $P_{O_2} = 4.2 \times 10^{-4}$ mbar, $P_{H_2} = 1.3 \times 10^{-4}$ mbar) is ~28 kJ/mol. The higher activation energy (E_a ~ 28 kJ/mol) as compared to value (E_a) in [21] is explained by the fact that the reaction rate was measured in excess oxygen partial pressure (the platinum surface was covered with an O_{ads}-layer).

The above results demonstrate that two kinetic regimes can be observed on platinum: (1) at $P_{O_2} > P_{H_2}$, the reaction rate is given by the expression $w = kP_{H_2}^2 P_{O_2}^{-1}$; (2) at $P_{O_2} < P_{H_2}$, the reaction rate is $w = kP_{O_2}$ [21]. Figure 5 shows that three reaction regions can be distinguished: oxygen side (O_{ads}), transition point (bistability) and hydrogen side (H_{ads}). The transition point $\theta_O \longrightarrow \theta_H$) occurs in a very narrow range of P_{H_2}, in which the surface wave appear (Fig. 6). At the initial reaction steps the Pt-tip surface is precovered with oxygen layer ($P_{O_2} = 5 \times 10^{-4}$ mbar) and the medium brightness of FIM image is mainly formed by O_2^+ ions (Fig. 6a). When hydrogen is introduced to the

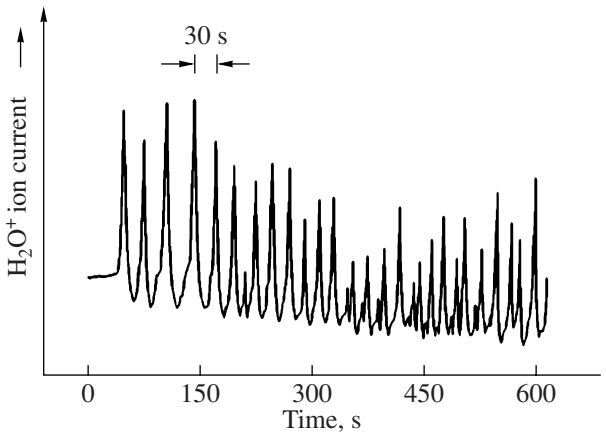

Fig. 7. Oscillatory behavior of the rate H_2O formation (H_2O^+) in H_2 oxidation on the Pt-tip at 300 K and $P_{O_2} = 5 \times 10^{-4}$ mbar, $P_{H_2} = 7 \times 10^{-4}$ mbar with an oscillation cycle of 30 s.

transition point ($P_{H_2} = 6 \times 10^{-4}$ mbar) the bright reaction front moves from upper right corner (Fig. 6a), which is imaged here by O_2^+ ions being formed near the metal surface from the desorbing H_2O molecules. The reaction begins on the {331} plane and propagates rapidly as a wave toward the (001) plane. Moving anisotropically, the wave flashes through the entire (001) plane within a short time interval of 0.12 s (Fig. 6b). The character of wave propagation anisotropy can clearly be seen in the FIM image presented in Fig. 6c: the wave moves rapidly in the (001) ⟶ (011) direction and slowly in the (001) ⟶ (112) direction. The image brightness of H_2O^+ ions, which is observed in 0.36 s (Fig. 6d), indicates that under the reaction wave propagation, a uniform, catalytically active surface is formed with high turnover frequencies. Based on ionization potential values ($I_{H_2O} \sim I_{O_2} < I_{H_2}$), we expected that, under the reaction conditions (300 K < T < 450 K, $P_{H_2} \sim 10^{-4}$ mbar, $P_{O_2} \sim 10^{-4}$ mbar), the surface-imaging gas would be O_2 (O_2^+) or H_2O (H_2O^+). It was shown that H_2O^+/H_3O^+ ions are the main ionic species, which serve as the imaging gas of the platinum surface in FIM [32].

According to field ion appearance energy spectroscopy measurements for H_2O^+/H_3O^+ ions [33], H_2O^+ ions being formed near the tip surface ($X_c \sim 4$ Å) from the desorbing reaction product (H_2O molecules) into the gas phase, whereas the formation of H_3O^+ ions can occur during a field-induced surface reaction for a protonation pathway involving H_{ads} and H_2O_{ads}: $H_{ads} + H_2O_{ads} \xrightarrow{\text{field}} H_3O^+$ [32, 33].

Following the experimental data water molecules are formed through a sequence of five reaction steps (in field-free conditions):

$$H_{2(g)} + 2* \longleftrightarrow 2H_{ads}, \quad \text{(I)}$$

$$O_{2(g)} + 2* \longrightarrow 2O_{ads}, \quad \text{(II)}$$

$$O_{ads} + H_{ads} \longrightarrow OH_{ads} + *, \quad \text{(III)}$$

$$H_{ads} + OH_{ads} \longrightarrow H_2O_{ads} + *, \quad \text{(IV)}$$

$$H_2O_{ads} \longrightarrow H_2O_{(g)} + *. \quad \text{(V)}$$

The applied electric field ($F \sim 1.2$ V/Å) introduces new reaction channels (steps VI–VII) that attributed to the surface imaging by H_2O^+/H_3O^+ ions:

$$H_2O_{(g)} \xrightarrow{\text{electric field}} H_2O^+_{(g)} + e^-_M, \quad \text{(VI)}$$

$$H_{ads} + H_2O_{ads} \xrightarrow{\text{electric field}} H_3O^+_{(g)} + e^-_M. \quad \text{(VII)}$$

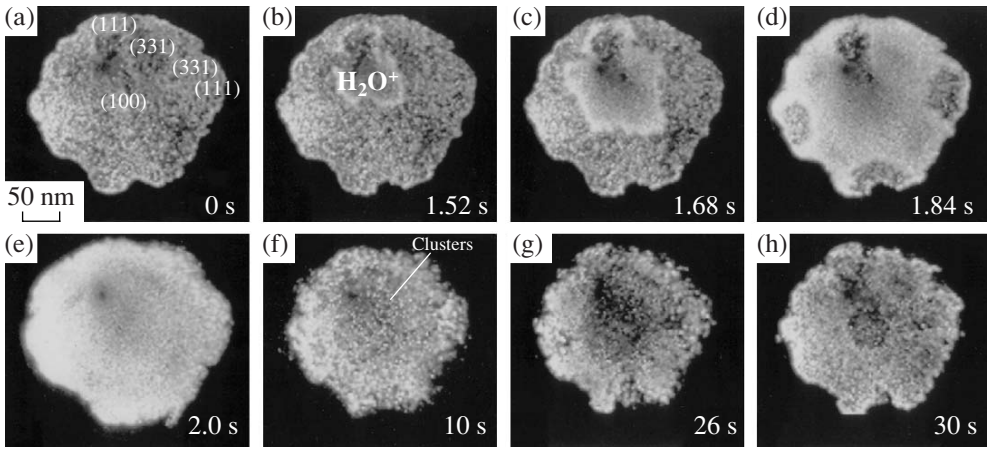

Fig. 8. FIM images showing initiation and wave propagation during the H_2 oxidation at 300 K on the Pt-tip surface at 300 K, $P_{O_2} = 5 \times 10^{-4}$ mbar, and $P_{H_2} = 7 \times 10^{-4}$ mbar. The time internals after the initial image ($\tau = 0$ s) is given at the lower right corners of the images.

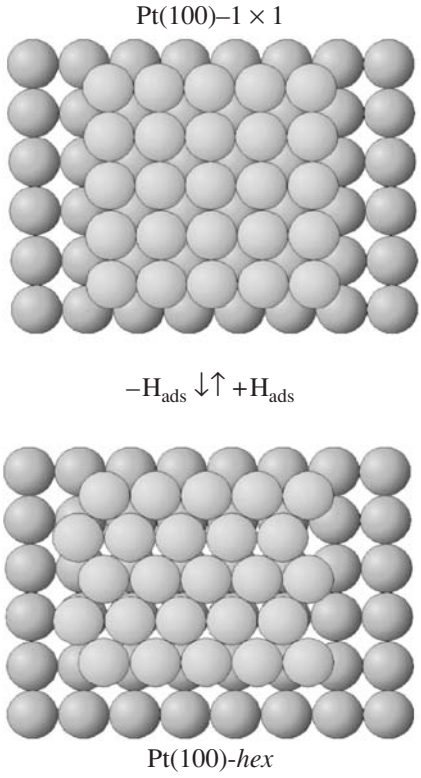

Fig. 9. Plan view of the Pt(100) single crystal shows the atomic structure on the reconstructed (100)-(hex) and unreconstructed (100)-(1 × 1) surfaces during the (*hex*) ⟶ (1 × 1) phase transition induced by H_2 adsorption.

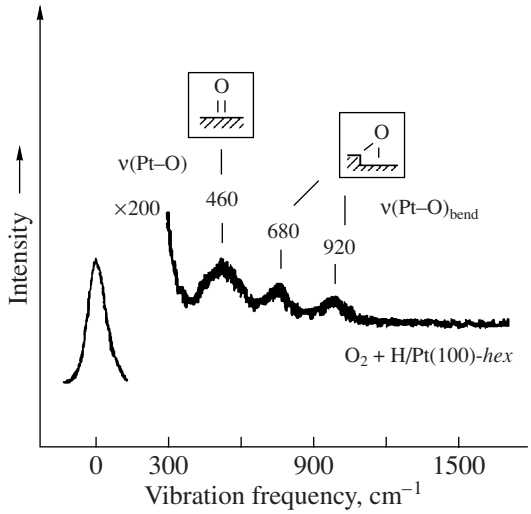

Fig. 10. Electron energy loss spectrum for atomic oxygen layer (O_{ads}) on the defects of the Pt(100)-(1 × 1) surface as a result of the $O_2 + H_{ads} \longrightarrow O_{ads} + H_2O$ titration reaction at 220 K. The oxygen exposure is 30 L.

The field induced routes are very fast (steps VI–VII) in comparison with chemical steps (I–V). Hence, in a unique fashion the temporarily catalytically active sites could be identified at a near-atomic resolution.

Self-Sustained Oscillations: Surface Waves

Figure 7 presents an example of regular isothermal self-sustained oscillations of the H_2O (H_3O^+) formation rate with an oscillation period of 30 s in H_2 oxidation on a Pt-tip at 300 K [9]. Figure 8 shows a sequence of FIM images for hydrogen oxidation at $T = 300$ K, $P_{O_2} = 5 \times 10^{-4}$ mbar, and $P_{H_2} = 7 \times 10^{-4}$ mbar under self-oscillation conditions [34]. The brightness of these images characterizes the variation of the state of the platinum surface. The areas with medium brightness represent O_{ads} layer imaged by O_2^+ ions (Fig. 8a). The very bright regions indicate areas with a high production rate of H_2O molecules (H_2O^+), which are ionized by the electric field, near the metal surface (Fig. 8e). The dark areas are covered by H_{ads} layer (Fig. 8f; image is obtained in O_2^+ ions).

As seen from the FIM study, the H_2O wave initiation on the O_{ads}-layer (Fig. 8a) start on the (100) nanoplane (Fig. 8b), which has spatial dimensions of ~400 Å. This wave spreads rapidly over the whole tip surface within <2 s (Figs. 8c–8e): from the (100) nanoplane toward the {110} nanoplanes at this stage. The reverse-traveling H_2O wave propagates over H_{ads}-layer more slowly (Figs. 8f–8h). The initial oxygen layer (Fig. 8a) is restored in 30 s, the time equal to the oscillation cycle.

In terms of the "phase transition" model, which was suggested in [3, 4], the formation of traveling waves (Fig. 8) can be explained as follows. The oscillation cycle (30 s) start with an O_{ads}-layer of the unreconstructed Pt(100)-(1 × 1) nanoplane (Fig. 8a) [35] that shows the formation of a highly reactive zone in the central (100) plane (Fig. 8b). This zone spreads rapidly over the whole surface (Figs. 8b–8e). Due to the high reactivity of the Pt(100)-(1 × 1) surface, the coverages of both reacting species (H_{ads} and O_{ads}) become rather low, resulting in nearly clean surface. As a consequence, the (1 × 1)-surface is no longer stable but transforms into the stable hexagonal phase (Fig. 8f).

Because the sticking coefficient for O_2 is much lower on the Pt(100)-(*hex*) surface ($S_0 \sim 10^{-3}$), build-up of a H_{ads}-layer takes place resulting in the partial lifting of the hexagonal reconstruction back to the (1 × 1)-phase [36]. The phase transition of the Pt(100)-(*hex*) into the Pt(100)-(1 × 1) surface is combined with a change in the density of the top Pt layer and during this process about 20% of its atoms are ejected. This process is visible in situ and manifests itself by the appearance of fluctuating small Pt clusters (brighter spots) that can be discerned in the image (Fig. 8f). The stepped (331) planes present on the tip surface, which have a high oxygen sticking coefficient, are new centers at which the reverse-traveling wave originates to propagate toward the central (100) plane. At this point in

time, the (100) plane is completely transformed into the (1×1) structure (Figs. 8g, 8h). The H_{ads} regions still appear as a dark area in the FIM images and shrink in diameter (Figs. 8g, 8h), until the surface is again completely covered with reverse-traveling oxygen wave (g ⟶ a), thus completing the oscillation cycle. The transition of the Pt(100) surface from the reconstructed structure (*hex*) to the unreconstructed structure (1×1), which is represented as a model in Fig. 9, can be caused by low-temperature H_2 adsorption [37]. According to He scattering data [38], the resulting H/Pt(100)-(1×1) phase has structure defects as atomic steps, which strongly affect the adsorption properties of the Pt(100) surface. For example, the O_2 sticking coefficient of the Pt(100)-*hex* surface is $S_0 \sim 10^{-3}$ and that of the (1×1) surface is $S_0 \sim 0.6$ [37]. According to our HREELS data, the O_{ads}-layer resulting from the $O_{2(g)} + H_{ads} \longrightarrow H_2O_{(g)} + O_{ads}$ reaction on the Pt(100)-(1×1) single crystal surface confirms the presence of a high concentration of surface defects. Figure 10 shows that interaction of an atomic hydrogen layer with oxygen (30 L) at 220 K is accompanied by the formation of an oxygen adatom layer with Pt–O bond vibration frequencies at 460, 680 and 920 cm^{-1}. In agreement with O^2/Pt(321) [39] the bands at 680 and 920 cm^{-1} are intrinsic to atomic states of oxygen on the structural defects (presumably like steps or kinks).

Our FIM/ HREELS results have strongly suggested that the H_{ads}-induced (*hex*) ⟷ (1×1) phase transition observed on the Pt(100) single crystal is the driving force for the isothermal oscillations found on that (100) surface:

$$\text{Pt-}hex \xrightarrow{+H_2} \text{H/Pt}{-}1 \times 1 \xrightarrow{+O_2(-H_2O)} \text{O/Pt}{-}1 \times 1$$
$$\xrightarrow{+H_2(-H_2O)} \text{Pt}{-}1 \times 1 \xrightarrow{\text{phase transition}} \text{Pt-}hex.$$

CONCLUSIONS

The nucleation and propagation of surface waves that are periodically emitted from a small nanoplane, was observed by FIM with a resolution of ~ 5 Å for the first time in the $H_2 + O_2$ (1 : 1) reaction on Pt-tips at a total pressure of 10^{-3} mbar.

Using the reaction product (H_2O molecules) as the imaging gas (H_2O^+), we related the appearance of regular waves with reaction rate oscillations. The initiating role is connected with the reversible phase transition (*hex*) ⟷ (1×1) of the Pt(100) nanoplane, which is the nucleation center of propagating waves on the Pt-tip. The periodic transition of platinum from the inactive state to the catalytically active state is due the reversible phase transition (*hex*) ⟷ (1×1) of the Pt(100) nanoplane induced by hydrogen adsorption. It has been found that the Pt(100) surface switches reversibly from an inactive state (*hex*) into a highly active state (1×1) under self-oscillation conditions. It has been established that the low activity (*hex*)-phase exhibited a low sticking coefficient for oxygen (S_{O_2}). The high activity of (1×1) surface has a high sticking coefficient (S_{O_2}) for oxygen and an increased population of active atomic oxygen states (O_{ads}), as is a result of the existence of the surface defect sites, which appear on the Pt(100) surface during the phase transition.

The reaction proceeds via the L–H detailed mechanism in which adsorbed hydrogen atoms (H_{ads}) in the initial stage react with chemisorbed oxygen (O_{ads}) to form hydroxyls (OH_{ads}), which react with a second hydrogen atom to produce water.

The H_2O molecules resulting from step (VII) are desorbed and are ionized by the electric field at a distance of ~4 Å from the metal surface. It becomes possible to use the H_2O^+ ion intensity as a local test for the presence of highly catalytic active surfaces (nanoplanes). With FEM/FIM techniques, it is possible to visualize, with a spatial resolution of ~2–20 Å, the active centers distribution on metal tips (~10^3 Å) whose size is comparable with the real size of the highly-dispersed supported metal catalysts (~300 Å). The most exciting result of this work that reveal the detailed mechanism of self-organization in $H_2 + O_2$ oscillating reaction on catalytically active surfaces of hundred angstroms size, lies in the following: the propagation of reaction–diffusion waves includes the participation of the different crystal nanoplanes and indicates an effective coupling of adjacent planes. Here, self-organization is understood as the spontaneous formation of stable spatiotemporal patterns (chemical waves) in non-equilibrium dissipative media.

ACKNOWLEDGMENTS

This work was supported by the Russian Foundation for Basic Research, grant no. 08-03-00454.

REFERENCES

1. Zhabotinsky, A.M., *Kontsentratsionnye avtokolebaniya* (Concentration Self-oscillations), Moscow: Nauka, 1974.
2. Nicolis, G. and Prigogine, I., *Self-Organization in Non-Equilibrium Systems*, New York: Wiley-Interscience, 1977.
3. Ertl, G., *Advances in Catalysis*, 1990, vol. 37, p. 213.
4. Imbihl, R. and Ertl, G., *Chem. Rev.*, 1995, vol. 95, no. 3, p. 697.
5. Gorodetskii, V.V. and Savchenko, V.I., *Proc. Fifth Int. Congr. on Catalysis*, Amsterdam: North-Holland, 1973, vol. 1, p. 527.
6. Gorodetskii, V.V., Sobyanin, V.A., Bulgakov, N.N., and Knor, Z., *Surf. Sci.*, 1979, vol. 82, p. 120.
7. Gorodetskii, V.V., Nieuwenhuys, B.E., Sachtler, W.M.H., and Boreskov, G.K., *Appl. Surf. Sci.*, 1981, vol. 7, p. 355.
8. Gorodetskii, V., Drachsel, W., Ehsasi, M., and Block, J.H., *J. Chem. Phys.*, 1994, vol. 100, no. 9, p. 6915.

9. Gorodetskii, V., Block, J.H., and Drachsel, W., *Appl. Surf. Sci.*, 1994, vol. 76/77, p. 129.
10. Boreskov, G.K., *Teoreticheskie problemy kataliza* (Theoretical Problems of Catalysis), Novosibirsk, 1977.
11. Norton, P.R., *J. Catal.*, 1975, vol. 36, p. 211.
12. Morrow, B.A. and Ramamurthy, P., *J. Phys. Chem.*, 1973, vol. 77, p. 3052.
13. Collins, D.M., Lee, J.B., and Spicer, W.E., *J. Vac. Sci. Technol.*, 1976, vol. 13, p. 266.
14. Mitchell, G.E. and White, J.M., *Chem. Phys. Lett.*, 1987, vol. 135, p. 84.
15. Gurney, B.A. and Ho, W., *J. Chem. Phys.*, 1987, vol. 87, p. 5562.
16. Müller, E. W. and Tsong, T. T. *Field–Ion Microscopy: Principles and Applications.* New York: Elsevier, 1969.
17. Suchorski, Yu., Imbihl, R., and Medvedev, V.K., *Surf. Sci.*, 1998, vol. 401, p. 392.
18. Sieben, B., Suchorski, Yu., Bozdech, G., and Ernst, N., *Z. Phys. Chem.*, 1997, vol. 202, p. 103.
19. Block, J.H., Drachsel, W., Ernst, N., Gorodetskii, V., and Sieben, B., *Ber. Bunsen-Ges. Phys. Chem.*, 1995, vol. 99, no. 11, p. 1363.
20. Gorodetskii, V.V., Matveev, A.V., Podgornov, E.A., and Zaera, F., *Top. Catal.*, 2005, vol. 32, nos. 1–3, p. 17.
21. Gorodetskii, V.V., Sobyanin, V.A., Cholach, A.R., and Smirnov, M.Yu., *Proc. 8th Int. Congr. on Catalysis*, West Berlin: Chemie, 1984, vol. 3, p. 323.
22. Gorodetskii, V.V., Elokhin, V.I., Bakker, J.W., and Nieuwenhuys, B.E., *Catal. Today*, 2005, vol. 105, p. 183.
23. Gorodetskii, V.V., Smirnov, M.Yu., and Cholach, A.R., in *"New Frontiers in Catalysis," 10th Int. Congr. on Catalysis*, Guczi, l., Solymosi, F., and Tetenyi, P., Eds., Amsterdam: Elsevier, 1993, part B, p. 1587.
24. Anton, A.B. and Cadogan, D.C., *J. Vac. Sci. Technol., A*, 1991, vol. 9, p. 1890.
25. Germer, T.A. and Ho, W., *Chem. Phys. Lett.*, 1989, vol. 163, p. 449.
26. Verheij, L.K. and Hugenschmidt, M.B., *Surf. Sci.*, 1995, vol. 324, p. 185.
27. Fisher, G.B. and Sexton, B.A., *Phys. Rev. Lett.*, 1980, vol. 44, p. 683.
28. Smirnov, M.Yu., Gorodetskii, V.V., Cholach, A.R., and Zemlyanov, D.Yu., *Surf. Sci.*, 1994, vol. 311, p. 308.
29. Gland, J.L., Sexton, B.A., and Fischer, G.B., *Surf. Sci.*, 1980, vol. 95, p. 587.
30. Carley, A.F., Davies, P.R., Roberts, M.W., and Thomas, K.K., *Surf. Sci.*, 1990, vol. 238, p. L467.
31. Sobyanin, V.A., Boreskov, G.K., and Cholach, A.R., *Dokl. Akad. Nauk SSSR*, 1984, vol. 279, p. 1410.
32. Drachsel, W., Wesseling, C., and Gorodetskii, V., *J. Phys. IV*, 1996, vol. 6, no. C5, p. 31.
33. Ernst, N., Bozdech, G., Gorodetskii, V., and Block, J.H., *Int. J. Mass Spectrom. Ion Processes*, 1996, vol. 152, p. 185.
34. Gorodetskii, V., Lauterbach, J., Rotermund, H.-H., Block, J.H., and Ertl, G., *Nature*, 1994, vol. 370, p. 276.
35. Barteau, M.A., Ko, E.I., and Madix, R.J., *Surf. Sci.*, 1981, vol. 102, p. 99.
36. Norton, P.R., Davies, J.A., Creber, D.K., Sitter, C.W., and Jackmann, T.E., *Surf. Sci.*, 1981, vol. 108, p. 205.
37. Norton, P.R., Davies, J.A., Jackson, D.P., and Matsunami, N., *Surf. Sci.*, 1979, vol. 85. p. 269.
38. Romainczyk, Ch., Manson, J.R., Kern, K., Kuhnke, K., David, R., Zeppenfeld, P., and Gomsa, G., *Surf. Sci.*, 1995, vol. 336, p. 362.
39. Gland, J.L., McClellan, M.R., and McFeely, F.R., *J. Chem. Phys.*, 1983, vol. 79, p. 6349.